Freeze Drying with Dielectric-Material-Assisted Microwave Heating

Wei Wang and Guohua Chen
Dept. of Chemical Engineering, The Hong Kong University of Science and Technology, Clear Water Bay, Kowloon, Hong Kong

DOI 10.1002/aic.11336
Published online October 29, 2007 in Wiley InterScience (www.interscience.wiley.com).

Experimental and theoretical investigations were conducted with regard to the effects of a dielectric material on freeze drying with microwave heating. The experimental results show that the dielectric material can effectively enhance the microwave freeze drying process, and substantial drying time can be saved compared with conventional freeze drying under the operating conditions tested. Theoretical study was performed by numerically solving a heat and mass transfer model of freeze drying with hygroscopic effect using the finite difference method with a moving boundary. The simulation results demonstrate the effectiveness of using the dielectric material in microwave freeze drying, especially when the solid content of the solution to be freeze dried is very low or the solid product has a very small loss factor. Comparisons of the drying curves display good agreements between experimental measurements and model predictions. Based on the profiles of the ice saturation and temperature, mechanisms of heat and mass transfer inside the material were analyzed, and the drying rate-controlling factor was discussed. © 2007 American Institute of Chemical Engineers *AIChE J,* 53: 3077–3088, 2007

Keywords: freeze drying, microwave, dielectric material, aqueous solution, simulation, heat transfer, mass transfer, mathematical modeling, porous media, drying

Introduction

Freeze drying plays an indispensable role among various drying techniques. There are many reasons why the freeze drying method is used to a great extent in industry. The most important one is that products freeze dried are most often sensitive to heat and cannot be dried with other techniques because of high operating temperatures. Freeze drying can be found in processing of food, pharmaceuticals, and biological products. In the food industry, a wide range of products including dairy products, meats, vegetables, and coffee are freeze dried.[1] In the pharmaceutical industry, the production process usually involves extraction, deposition, separation, and purification that usually lead to a dilute aqueous solution. Water is then removed by freeze drying, leaving the dried product to be packaged or further processed.[2] Freeze drying is also employed to preserve blood, bone, skin, and other labile biomaterials.[3]

In a freeze drying process, the major concerns are product quality and processing cost. It is well known that freeze drying produces the highest quality of products among all current drying techniques. Freeze drying has the advantages of protection against chemical decomposition, minimum loss of activity and easy rehydration of product due to the low processing temperature and reduction of moisture content to a very low value.[4] However, it is one of the most energy-consuming unit operations. The high energy consumption results not only from the phase change of moisture but also from the overall low energy efficiency of the process.[5] Conventional vacuum freeze drying is characterized by long drying time and high cost. Freeze drying combined with microwave heating has been proved, to some extent, to have the

Correspondence concerning this article should be addressed to G. Chen at kechengh@ust.hk.

advantages of reliability and high quality of conventional freeze drying, and fast drying rate and low cost of microwave heating.[6]

Early research of applying microwave energy in freeze drying concentrated on demonstrating its feasibility. Ma and Peltre[7] experimented with microwave freeze drying of slabs of raw beef. Ang et al.[8] used beef cubes as the materials examining the effects of electric field strength on freeze drying. Wang and Shi[9,10] experimentally compared traditional surface heating and microwave heating in freeze drying of raw beef. They found that drying time of using microwave was about 50% shorter than that of the traditional one. It is noticed that the materials used in those early studies were all the naturally formed solid materials. There are a few papers on freeze dehydration of liquid materials with microwave heating. Ben Souda et al.[11] presented an experimental study on microwave freeze drying of foamed milk, which found that excessive microwave power could cause the frozen materials to melt. Dolan and Scott[2] performed an experiment on vial microwave freeze drying of mannitol aqueous solution. A common feature of the two studies is that microwave heating had no great effects on the freeze drying process. The less attention paid to microwave freeze drying of aqueous solution may be due to a lack of sound understanding of the microwave heating mechanism. Microwave heating effect is recognized to be an interaction between microwave and lossy material, which results in part of the microwave energy to dissipate volumetrically in the form of heat. The quantification of microwave energy conversion depends strongly on the dielectric properties of the frozen mass, especially the loss factor. Since ice, unlike water, has a loss factor of 0.003, it hardly absorbs microwave energy. Solid matrix in the frozen material will therefore act as an internal heat source supplying energy needed for sublimation. When the loss factor of solid is small, microwave energy will not be effectively exerted on the material being dried. It is known that the dried meat has a relatively high loss factor, while solid milk and mannitol have very small values. This explains why an obvious reduction of drying time could be gained in microwave freeze drying of beef.

Microwave freeze drying is gaining a worldwide interest in both academic and industrial sectors. How to utilize this volumetric heating method in the freeze drying process while maintaining acceptable quality of the dried products still remains a challenge. To make use of microwave energy and also retain the advantages of vacuum freeze drying, Wang and Chen[6] have proposed microwave freeze drying of aqueous solution with the assistance of a dielectric material. A dielectric sphere or bar is first frozen with the solution to be dried, and the composite is then freeze dried with microwave heating. Theoretical studies conducted earlier have shown that the dielectric material can significantly enhance the microwave freeze drying process, and drying time can be greatly reduced.[12–14] Meanwhile, similar numerical analyses by Basak and Priya[15,16], Basak et al.[17], and Basak and Meenakshi[18] have demonstrated high efficiencies for the microwave heating of one-dimensional food samples (oil and beef) placed on dielectric ceramic supports [Al_2O_3 and silicon carbide (SiC)]. The improved heating was illustrated in terms of the average power absorbed vs. sample thickness, and generalized heating strategies using uniform plane waves were derived. It is now necessary to verify this new, interesting, and also industrially relevant technique experimentally. The aims of the present study are to perform experimental studies to demonstrate the effects of the dielectric materials in microwave freeze drying, and to verify the model predictions with experimental measurements. This fundamental research is essential to optimize the process for the best combination of product quality and processing cost, and to provide a helpful tool for future design, operation, and control.

Apparatus

A laboratory scale microwave freeze drying apparatus was designed, made and assembled in this study. The overall system consists of five major units: vacuum unit, air heating unit, microwave unit, data acquisition unit, and freezing unit. Schematic diagram of the apparatus is given in Figure 1.

The vacuum unit consists of a drying chamber, a vacuum pump and a vapor condenser. A quartz bell jar (TGP, USA) about 2.3 L in volume was employed as the drying chamber. A vacuum pump (E2M18, BOC Edwards, UK) operated to give an initial purging rate of about 4.72 L/s and an ultimate vacuum of 0.1 Pa. A purpose-designed liquid nitrogen condenser (about 1.7 L) was used as a cool trap to prevent water vapor from entering the pump. The relatively large initial volume of the condenser also helped speed up the development of a vacuum at the beginning of the drying cycle. The ultimate 2 Pa pressure was developed within 4 min in the unit when the connections were well sealed.

The air heating unit includes a circulator (9710, PolyScience, USA), a heat exchanger and a blower. The circulator has a wide temperature range between $-45^{\circ}C$ and $200^{\circ}C$, high stability of $\pm 0.01^{\circ}C$ and a five-speed pressure and suction (duplex) pump. A stainless steel brazed plate heat exchanger (Qinbao, China) was selected for air–water heat exchanging. It has an area of 0.53 m^2, a design pressure of 1 MPa and design temperature ranging from -196 to $200^{\circ}C$. A ring blower (Crelec, Taiwan) has a power of 180 W, a flow rate of 48 m^3/h and a pressure head of 45 mbar. It was used for air circulation in an effort to adjust the air temperature and thereby to maintain a constant value of temperature on the jar surface.

The microwaves were generated in a modified commercial microwave oven (VIP2763, Whirlpool, China). Since there was no dummy load to release the reflected power or prevent the reflected power from returning to the power generator, the microwave power output must be lowered to match the sample quantity. Two modifications were made. First, the original Whirlpool magnetron of 1000 W was replaced by a Panasonic magnetron of 600 W; secondly, a transformer was employed to decrease the input voltage so as to lower the power output. The variation of microwave input power with voltage is shown in Figure 2. The minimum continuous input power is about 40 W in this oven.

In this drying system, three parameters, sample weight, vacuum pressure, and surface temperature of the bell jar were recorded during each drying run. The data acquisition unit includes three sensors, as well as a personal computer (PC) and a data acquisition card. An infrared sensor (Raytek CI3A, USA) was chosen to monitor the surface temperature of the glass bell jar. It is designed to measure accurately and

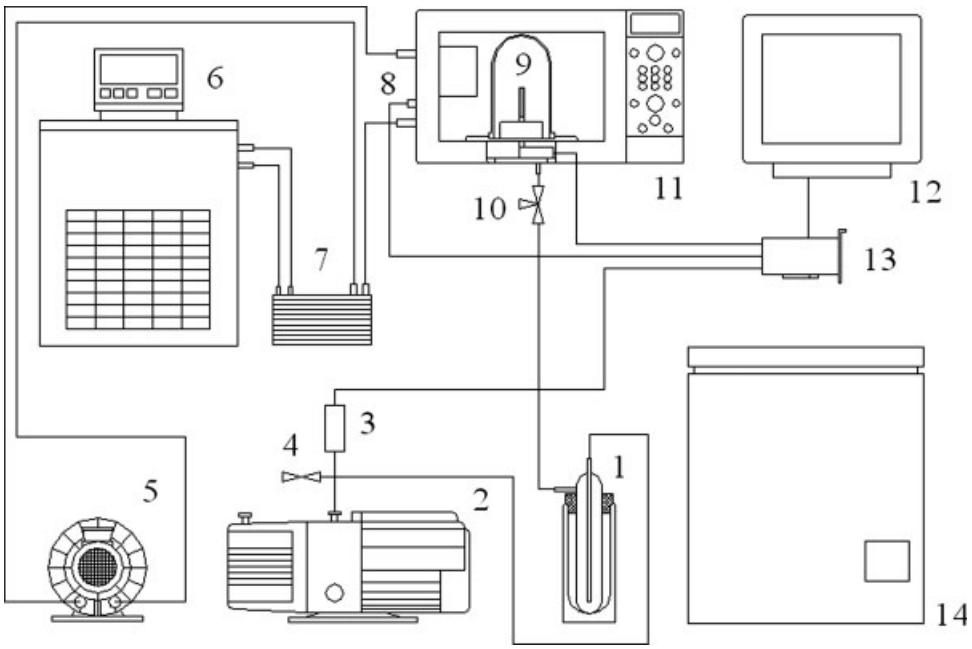

Figure 1. Schematic diagram of the microwave freeze drying apparatus.

1, Cool trap; 2, vacuum pump; 3, pressure sensor; 4, exhaust valve; 5, blower; 6, circulator; 7, heat exchanger; 8, infrared sensor; 9, drying chamber; 10, isolation valve; 11, microwave oven; 12, PC; 13, data acquisition card; 14, freezer.

repeatably the amount of heat energy emitted from the jar surface and to convert that energy into a measurable electrical signal. A loadcell (NTS Instrument, China) was mounted to measure the weight loss of the sample with time. It has a rated output of 1.5 mV/V (±10%). An amplifier was installed to convert the microvoltage signal into the voltage signal to fit the specified range of the data acquisition card. The vacuum pressure sensor used in this system is an active Pirani gauge (BOC Edwards, UK), a single compact unit combining a vacuum gauge with a gauge controller. All three signals were digitized by a data acquisition card and recorded with a PC. The IBM PC has a P4-1.7 GHz CPU and 384 MB RAM. The multifunctional data acquisition card (NI PCI-6221, USA) collected the sensors' readings representing load, pressure, and temperature through a relay connection block and digitized them for the computer to process. The computer stored and analyzed the signals using LabVIEW7.0 software.

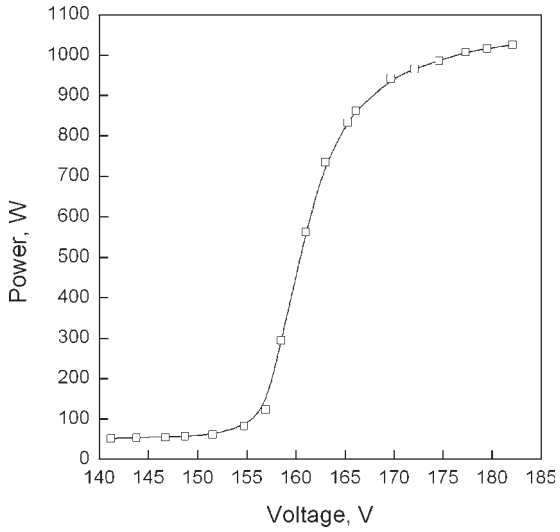

Figure 2. Variation of microwave input power with voltage.

The samples were frozen in an ultra low temperature freezer (BD-100LT, Haier, China) outside the drying chamber. This freezer has 100 L in capacity with a temperature adjustable from −20 to −40°C. To avoid an undesirable increase in temperature prior to the start of experiment, the frozen samples were moved into the drying chamber as quickly as possible, and the chamber was evacuated immediately. A microwave resistant rubber O-ring was fitted for sealing. This allowed quick mounting of the quartz bell jar on its support.

Experimental

Materials

Mannitol (Sigma–Aldrich, >98%) was selected as the solute in aqueous solution because it is an excellent pharmaceutical excipient in structure modifying with which the porous structure after freeze drying can be well retained and the chance of collapse can be greatly reduced.[19] Sintered SiC was used as the dielectric material in the experiments. It has a large loss factor similar to that of liquid water, which means that it is easy to absorb microwave energy. For a general discussion of the effect of loss factors on freeze drying, readers are referred to previous publications.[12,20,21] For com-

Table 1. Dielectric Materials Tested

Name	Loss Factor	Dimension, mm
Sintered silicon carbide	11	φ6 × 35
Quartz	0.003	φ6 × 35

parison, quartz was also used as a dielectric material to serve as a control case because it hardly absorbs microwave energy. The properties of the dielectric materials are listed in Table 1.

Sample preparation

The aqueous solution of mannitol was prepared by dissolving 5 g of mannitol powder in a beaker of 100 mL with 25 g of de-ionized water. The moisture content, X_0 (dry base), was 5 kg/kg corresponding to 83.33 wt % on wet base. The solution was poured into a mold to form a cylinder with a dielectric material rod at the center. Such a sample mold was then placed into the freezer until it was completely frozen and had reached the desired starting temperature. Figure 3 shows the schematic diagram of a sample to be dried. The cylindrical geometry was employed in this experimental study not only for matching the dimension of the freeze drying chamber but also for the future industrial application because this shape is convenient to form, and dried products can be easily separated from the dielectric material rod.

The porosity, ε, of the frozen material can be determined using the following formula:

$$\varepsilon = \frac{X_0 \rho_s}{X_0 \rho_s + S_0 \rho_i}. \tag{1}$$

The initial weight, W_{t0}, of the sample was obtained by weighing the sample with an electronic balance before each experiment. The weight of the solid material in a sample could then be calculated as:

$$W_s = \frac{W_{t0}}{1 + X_0}. \tag{2}$$

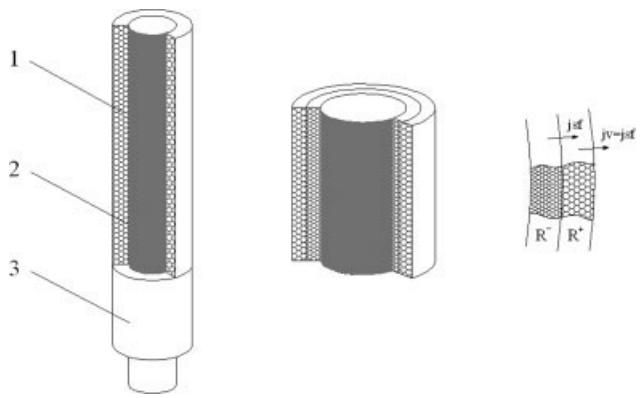

Figure 3. Schematic diagram of a sample.

1, Sample support; 2, dielectric material rod; 3, material to be dried.

Experimental Procedures

The experiments were divided into two operational modes, i.e., conventional freeze drying without microwave heating, and microwave heated freeze drying with and without the assistance of the dielectric material under ambient temperatures of 25 and 41°C, respectively.

In conventional freeze drying, a quartz rod was used as the core at the center of the cylindrical frozen sample. The test was carried out without microwave heating. The heat needed for freeze drying all came from radiation of the quartz bell jar toward the surface of the sample. An initial material temperature of −32°C was selected because the mannitol solution has the collapse temperature of −30°C.[22,23] In microwave heated freeze drying, either a quartz rod or an SiC rod was used as the core of the sample. With microwave heating, the heat for freeze drying was supplied not only by surface radiation but also by the volumetric energy of microwave. The operating conditions are summarized in Table 2. Since the two modes of operation are similar, only the experimental procedure of the latter one is described as follows

1) Turn on the blower and circulator (5 and 6 in Figure 1) to preheat the drying chamber to the desired temperature. Check the cool trap to make sure that liquid nitrogen is supplied.

2) Close the exhaust and isolation valves (4 and 10 in Figure 1). Turn on the vacuum pump to achieve an ultimate pressure of 2 Pa of the system before the glass bell jar (drying chamber).

3) Move the sample from the freezer quickly into the drying chamber, cover the bell jar on the bottom, and switch on the isolation valve.

4) Turn on the power supply of the microwave oven.

5) Record the sample weight, ambient temperature, and pressure at a given time interval with the data acquisition system.

6) Turn off the microwave power when there is no visual change in the sample weight displayed on the front panel where the ambient pressure shows going down to the initial value of about 2 Pa.

7) Turn off the vacuum pump; switch on the exhaust valve for ventilation.

8) Remove the sample and measure the weight of dried product to determine the residual moisture content.

The moisture content of the sample during drying is

$$X = \frac{W_t - W_s}{W_s}. \tag{3}$$

The moisture content can be expressed in terms of ice saturation using the following formula:

$$S = \frac{(1 - \varepsilon)\rho_s X}{\varepsilon \rho_i}. \tag{4}$$

Table 2. Operating Conditions

Variable	Value	Unit
d_p	6	mm
D_p	8.6	mm
P	40–50	W
S_0	1	–
T_0	−32	°C
T_{amb}	25/41	°C

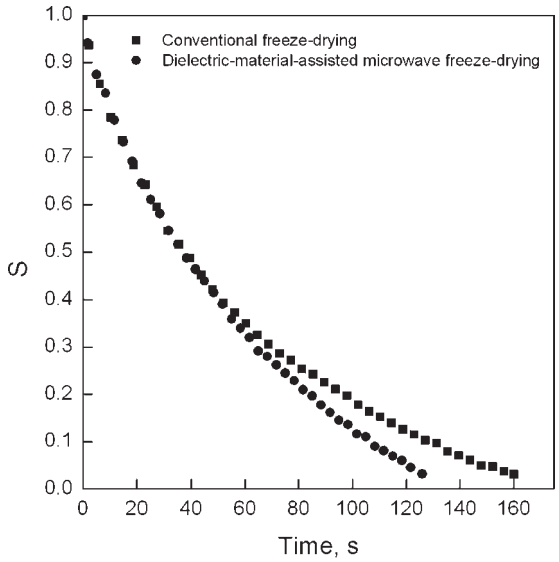

Figure 4. Experimental drying curves at 25°C.

This transformation allows easy comparisons between the experimental results and theoretical predictions discussed subsequently.

Experimental Results and Discussion

In each experiment, special attention was given to the measurement of drying curve. Variations of ambient temperature and vacuum pressure during drying were also recorded.

Figure 4 shows the drying curves for conventional freeze drying and dielectric-material-assisted microwave freeze drying at 25°C. It was attempted to replace the SiC rod with a quartz rod so as to show the effect of microwave heating without the assistance of the dielectric material. The absorption of microwave energy was so low that the reflected energy burnt the magnetron because there was no dummy load to absorb the reflected power in this arrangement. Thus, no experimental data could be collected on microwave freeze drying without dielectric material assistance. It can be seen in Figure 4 that the drying time was 126 min for dielectric-material-assisted microwave freeze drying, 21.3% shorter than 160 min required with conventional freeze drying. This indicates that dielectric-material-assisted microwave freeze drying is workable, and the use of the dielectric material in microwave freeze drying can indeed enhance the freeze drying process as predicted.[14]

Careful observation reveals that microwave heating seemed to take effect gradually. This is because the dielectric material rod had to absorb sufficient energy to increase its temperature first while the surface radiation was drying the sample. In addition, heat conducted from the dielectric material core had to pass through almost the entire thickness of the frozen material initially; meanwhile the radiation heat at the very beginning can easily be utilized for sublimation of ice. With the receding of the sublimation front, the heat conducted from the dielectric material increased while the surface radiation was not dominant; hence, the importance of the microwave heating became more pronounced at the latter half of drying.

Figure 5 shows the variation of ambient pressure inside the drying chamber. In conventional freeze drying, the pressure gradually decreased from the beginning to the end of drying. With dielectric-material-assisted microwave heating, the pressure remained roughly constant through most of the drying process, and then quickly decreased toward the end. This is because of the faster sublimation with microwave heating compared with conventional freeze drying. A dynamic balance of pressure was developed between the sublimation rate and purging rate with the given pump capacity. A short increase in pressure at the very beginning of the microwave-heated drying was caused by inertia effect due to a quick decrease in pressure. It is notable that the average pressures in the two cases were nearly the same.

Figure 6 shows the variations of ambient temperature inside the drying chamber. It can be seen that the temperature remained approximately constant.

For comparison, experiments were also carried out at 41°C with and without the aid of the dielectric material. Because the variations of pressure and temperature were similar to those shown in Figures 5 and 6, only drying curves are presented in Figure 7. The drying time with dielectric material assistance was 19.7% shorter than that without assistance. The slightly smaller enhancement seen in Figure 7 compared with Figure 4 is because of the lower ambient temperature for the case of Figure 4 where more of the energy came from microwave heating. Ice saturation in the dried products was below 0.03 in all four cases.

Mathematical Model

Governing equations

Since a saturated frozen material was used in this study, only one sublimation front is expected during drying, as shown in Figure 3. Movement of the sublimation front results in a partial removal of moisture due to hygroscopic effect.

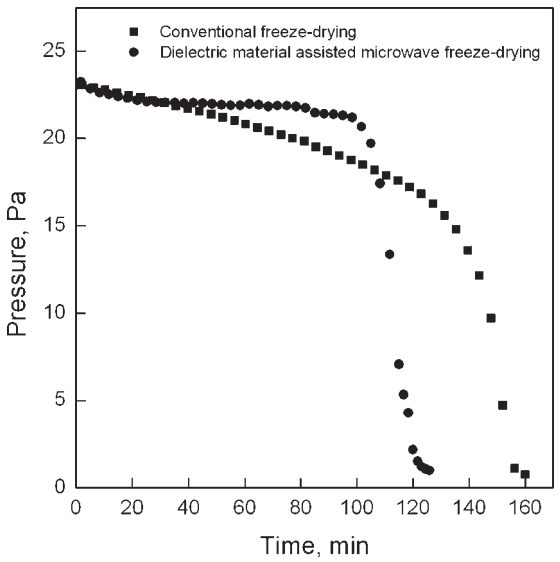

Figure 5. Measured chamber pressure at 25°C.

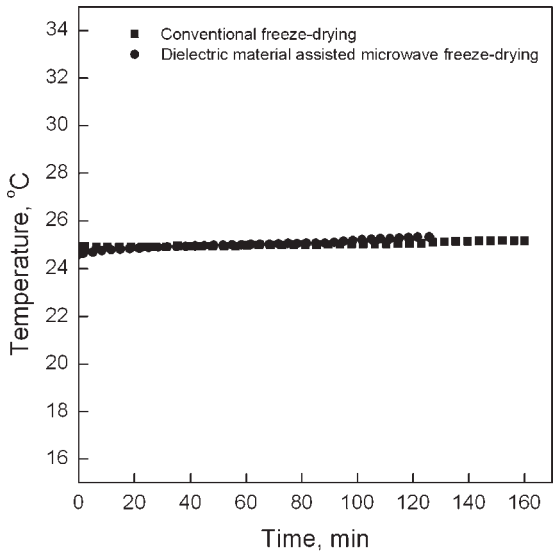

Figure 6. Measured ambient temperature.

The region receded after front movement is called the drying region, corresponding to the postfront-moving region described in a previous study.[13] There is a certain amount of moisture in adsorption–desorption equilibrium in this region. Comparably, the region before front movement is called the frozen region. The main assumptions made in the model development have been reported elsewhere.[13] The mathematical model equations used for this study are similar to those developed previously with the spherical coordinate system converted into a cylindrical one.

In the drying region, the vapor movement in the unsaturated region is recognized to be a pressure- and vapor-concentration-driven flow.[24] Based on Darcy's law, Fick's law and Fourier's law, the mass and heat conservation equations in this region can be derived as

$$\varepsilon\rho_{\mathrm{i}}\frac{\partial S}{\partial t}=\frac{1}{r}\frac{\partial}{\partial r}\left(rK_{\mathrm{S}}\frac{\partial S}{\partial r}\right)+\frac{1}{r}\frac{\partial}{\partial r}\left(rK_{\mathrm{T}}\frac{\partial T}{\partial r}\right), \tag{5}$$

$$K_{\mathrm{T}}=\frac{K_{\mathrm{D}}K_{\mathrm{r}}}{\mu_{\mathrm{v}}}R_{\mathrm{v}}\rho_{\mathrm{v}}^{2}+\left[\frac{K_{\mathrm{D}}K_{\mathrm{r}}}{\mu_{\mathrm{v}}}R_{\mathrm{v}}\rho_{\mathrm{v}}T+\frac{(1-S)\varepsilon}{\tau}D\right]\frac{\partial\rho_{\mathrm{v}}}{\partial T}, \tag{5a}$$

$$K_{\mathrm{S}}=\left[\frac{K_{\mathrm{D}}K_{\mathrm{r}}}{\mu_{\mathrm{v}}}R_{\mathrm{v}}\rho_{\mathrm{v}}T+\frac{(1-S)\varepsilon}{\tau}D\right]\frac{\partial\rho_{\mathrm{v}}}{\partial S}. \tag{5b}$$

$$\rho c\frac{\partial T}{\partial t}=\frac{1}{r}\frac{\partial}{\partial r}\left[r(\lambda+K_{\mathrm{T}}\Delta H)\frac{\partial T}{\partial r}\right]+\frac{1}{r}\frac{\partial}{\partial r}\left(rK_{\mathrm{S}}\Delta H\frac{\partial S}{\partial r}\right)+\dot{q}, \tag{6}$$

$$\rho c=(1-\varepsilon)\rho_{\mathrm{s}}c_{\mathrm{s}}+\varepsilon S\rho_{\mathrm{i}}c_{\mathrm{i}}+\varepsilon(1-S)\rho_{\mathrm{v}}c_{\mathrm{v}}, \tag{6a}$$

$$\lambda=(1-\varepsilon)\lambda_{\mathrm{s}}+\varepsilon S\lambda_{\mathrm{i}}+\varepsilon(1-S)\lambda_{\mathrm{v}}, \tag{6b}$$

$$\dot{q}=[(1-\varepsilon)k_{\mathrm{s}}+\varepsilon Sk_{\mathrm{i}}]E^{2} \tag{6c}$$

In the frozen region, there is no mass transfer, since the frozen material's voids are completely filled with ice crystals. Based on the local thermal equilibrium, the heat conservation equation can be expressed as

$$\rho c\frac{\partial T}{\partial t}=\frac{1}{r}\frac{\partial}{\partial r}\left(r\lambda\frac{\partial T}{\partial r}\right)+\dot{q}, \tag{7}$$

$$\rho c=(1-\varepsilon)\rho_{\mathrm{s}}c_{\mathrm{s}}+\varepsilon\rho_{i}c_{i}, \tag{7a}$$

$$\lambda=(1-\varepsilon)\lambda_{\mathrm{s}}+\varepsilon\lambda_{i}, \tag{7b}$$

$$\dot{q}=[(1-\varepsilon)k_{\mathrm{s}}+\varepsilon k_{\mathrm{i}}]E^{2}. \tag{7c}$$

In the dielectric material region, only heat transfer takes place. The heat conservation equation is

$$\rho c\frac{\partial T}{\partial t}=\frac{1}{r}\frac{\partial}{\partial r}\left(r\lambda\frac{\partial T}{\partial r}\right)+\dot{q}, \tag{8}$$

$$\rho c=\rho_{\mathrm{m}}c_{\mathrm{m}}, \tag{8a}$$

$$\lambda=\lambda_{\mathrm{m}}, \tag{8b}$$

$$\dot{q}=k_{\mathrm{m}}E^{2}. \tag{8c}$$

Boundary conditions

At the cylindrical axis, there is no heat flux,

$$\left.\frac{\partial T}{\partial r}\right|_{r=0}=0. \tag{9}$$

On the surface of the dielectric material core, there is no mass flux,

$$\left.\frac{\partial S}{\partial r}\right|_{r=r_{\mathrm{p}}}=0. \tag{10}$$

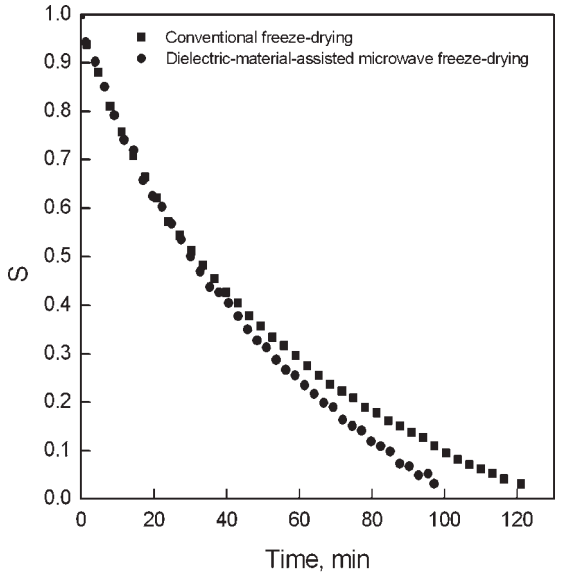

Figure 7. Experimental drying curves at 41°C.

On the surface of the sample, the heat transfer is governed by radiation, and the drying chamber has a constant pressure,

$$q\Big|_{r=R_p} = \sigma e F \left(T^4\Big|_{r=R_p} - T_{amb}^4 \right), \tag{11}$$

$$\rho_v\big|_{r=R_p} = \frac{P_{amb}}{R_v T\big|_{r=R_p}}. \tag{12}$$

At the sublimation front, the vapor flux is

$$j_{sf} = -\varepsilon(S - S_{ini})\rho_i \frac{dR}{dt}\bigg|_{R^-}. \tag{13}$$

The mass and heat balance equations are

$$j_v\big|_{R^+} = j_{sf}, \tag{14}$$

$$q\big|_{R^-} - q\big|_{R^+} = j_{sf}\Delta H. \tag{15}$$

Initial conditions

The initial distributions of the temperature and the ice saturation are uniform. The sublimation front starts from the sample surface.

$$T\big|_{t=0} = T_0, \tag{16}$$

$$S\big|_{t=0} = S_0, \tag{17}$$

$$R\big|_{t=0} = R_p. \tag{18}$$

Numerical Simulation

Properties to consider

In freeze drying, molecular diffusion and Knudsen diffusion are considered the dominant transport mechanisms. Compared with molecular diffusion, Knudsen diffusion is the controlling step in vapor diffusion in a porous medium, because the mean free path of the molecules is much larger than the average pore radius.[12] Knudsen diffusivity can be written as[25]

$$D = \frac{97.0\bar{r}\varepsilon}{\tau}\sqrt{\frac{T}{M_w}}, \tag{19}$$

where the average pore radius, $\bar{r}$, of dried porous product was assumed to be 2.65×10^{-6} m according to the experimental datum of a similar material.[26]

Based on the assumption of a rigid porous medium, the intrinsic permeability is unchangeable. However, porosity is variable in the drying region where it is partially saturated with ice crystals. The material permeability increases as the moisture content decreases due to the development of additional void space. According to Nield and Bejan,[27] the relative permeability is

$$K_r = 1 - S. \tag{20}$$

In a hygroscopic porous material with bound moisture, it is recognized that the thermodynamic equilibrium relationship should be replaced by an adsorption equilibrium relationship. However, such a relationship has not been developed either theoretically or experimentally at ultra low temperatures. A simple adsorption–desorption equilibrium relationship was utilized in a recent theoretical study.[13] Because of the combination of moisture with the porous solid, the tendency of the moisture to escape is apparently smaller than that of a pure fluid, and the maximum vapor pressure in the adsorption equilibrium is equal to that in thermodynamic equilibrium. The previous study has proposed that the ratio of vapor pressures between the adsorption equilibrium and the thermodynamic equilibrium follows a linear relation, in other words equal to the moisture saturation, S.[13] This is similar to the modified Antoine equation recommended by Do.[28] In this simulation, a more generalized form of the ratio was adopted through a small modification of the previous relation as follows:

$$\frac{P_v(T,S)}{P_v(T)} = S^{\frac{1}{\alpha}}. \tag{21}$$

where the value of parameter, α, may depend on the materials and operating conditions. It should be pointed out that the adsorption–desorption equilibrium is always assumed to be valid throughout the drying process, as proposed by Ni et al.[29] and Chen et al.[30] This avoids a discontinuous first-order derivative of the vapor mass concentration in a situation where either the adsorption equilibrium or the thermodynamic equilibrium might be used.

The emissivity, e, is regarded as the porosity, and the angle factor, F, is considered to be unity following Bird et al.[31] Specific values of all the properties can be found in Table 3.

Table 3. Properties Used in the Simulation

Symbol	Value	Unit	References
c_i	1930	J/(kg K)	32
c_m	715	J/(kg K)	33
c_s	1310	J/(kg K)	34
c_v	1886	J/(kg K)	32
ΔH	2.839×10^6	J/kg	34
K_D	3.62×10^{-10}	m^2	26
k_i	4.09×10^{-4}	$W/m^3\ (V/m)^{-2}$	35
k_m	1.5	$W/m^3\ (V/m)^{-2}$	33
k_s	2.13×10^{-3}	$W/m^3\ (V/m)^{-2}$	6
S_{ini}	0.06	–	26
ε	0.8907	–	Experimental section
ε_0	8.854×10^{-12}	F/m	35
λ_i	2.22	J/(s m K)	32
λ_m	114	J/(s m K)	33
λ_s	1.06	J/(s m K)	36
λ_v	0.022	J/(s m K)	32
μ_v	$0.011 \times (T/273)^{1.5}/(T+961)$	kg/(m s)	37
ρ_i	913	kg/m^3	32
ρ_m	3160	kg/m^3	33
ρ_s	1489	kg/m^3	6
σ	5.576×10^{-8}	$W/(m^2\ K^4)$	31
τ	1.2	–	26

Numerical procedure

In the primary drying stage, governing Eqs. 5–8, together with the initial and boundary conditions of Eqs. 9–18 were solved numerically using the finite-difference method with an internal moving boundary. A variable time-step in the global domain was adopted in this simulation. Sublimation at the front was considered to take place within the grid of the frozen region very near the front in each time increment. In the secondary drying stage, only Eqs. 5, 6, and 8 were solved without the moving boundary and the frozen region, since the whole sample volume becomes the drying region.

The source-term was treated into a general form as

$$S_t = S_C + S_P \Phi_P, \tag{22}$$

where S_C stands for the constant part of S_t, while S_P is the coefficient of Φ_P. In this simulation, the source-term was linearized by setting the entire S_t into S_C with S_P being equal to zero. This approach is practicable and perhaps the only choice when the expression of S_t is very complicated[38] in the present situation although the CPU occupied time would be a bit longer.

The control-volume method with the fully implicit scheme was used for discretization. The cell-centered scheme was adopted, i.e., grid nodes were placed at the geometric centers of control-volumes because there was a sudden change in physical properties between the different regions of the material. Governing Eqs. 5–8 were discretized into a general form of linear algebraic equations as

$$a_P \Phi_P = a_E \Phi_E + a_W \Phi_W + b, \tag{23}$$

where Φ denotes the generalized independent variable, T or S. Since the coefficients, a_P, a_E, a_W, and the source-term, b, depend on T and S, iteration is necessary. Within each time-step, the procedure involved the following steps:

1) Start with a guess or an estimate for the values of Φ at all grid points.

2) From these guessed, Φs, calculate tentative values of coefficients and the source-term.

3) Solve the nominally linear set of algebraic equations to get new values of Φ.

4) With these Φs as better guesses, return to step 2 and repeat the procedure until further repetitions (iterations) cease to produce any significant changes in the values of Φ.

An under-relaxation was employed to avoid divergence in iterative solutions of such strongly nonlinear equations. The discretized equations were solved using the tridiagonal-matrix algorithm.[38] During simulation, a significantly fine grid was applied to obtain a precise solution. The convergence criteria of iterations are as follows:

$$\sum_{l}^{n_T} \frac{\mathrm{abs}\left(T_l^j - T_l^{j-1}\right)/T_l^j}{n_T} < 10^{-8}, \tag{24}$$

$$\sum_{l}^{n_S} \frac{\mathrm{abs}\left(S_l^j - S_l^{j-1}\right)/S_l^j}{n_S} < 10^{-8}. \tag{25}$$

Simulation Results and Discussion

Comparisons between experimental and simulated drying curves

During simulation, the linear relation of the ratio of vapor pressures between the adsorption equilibrium and the thermodynamic equilibrium ($\alpha = 1$) was first used for conventional freeze drying at 25°C of the ambient temperature. This yielded a large difference between the theoretical prediction and the experimental data. The simulation overestimated the experimental drying curve. Moreover, the simulation ended at about 0.12 of saturation and further reduction could not be induced. This is because the surface pressure in porous medium was very close to the saturated vapor pressure in adsorption equilibrium without ice sublimation and vapor transport.

It is known that two points of the ratio given in Eq. 21 can be determined for any hygroscopic material: 0 for the dried product ($S = 0$), and 1 for pure ice ($S = 1$). The overestimation reveals that the ratio must be above S. Since S ranges from 0 to 1, α is above 1. Ideally, the value of α should be determined by fitting the experimental results to the theoretical analysis. However, for the simulation program to work, a value of α has to be known first. Hence, trial and error is needed. For simplicity, 2 and 3 of αs were tested respectively in the next logic trials. Figure 8 shows the two resulting predicted drying curves together with the case of $\alpha = 1$. It was very surprising and rewarding to find that the agreement between the theoretical analysis and the experimental result was very good for $\alpha = 2$, as shown in Figure 9. It is worth emphasizing that the theoretical predictions here were all based on the real physical properties of the materials and fundamental laws of transport phenomena with only one proposed equilibrium equation describing the hygroscopic effect of the material of interest. For the case where α equals 3, the simulation underestimated the experimental drying curve with the drying time shorter by about 15% than the experimental results, as seen in Figure 8.

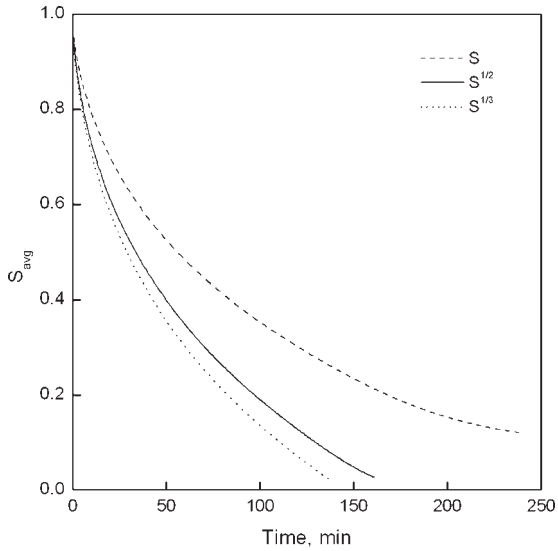

Figure 8. Predicted drying curves with different relations.

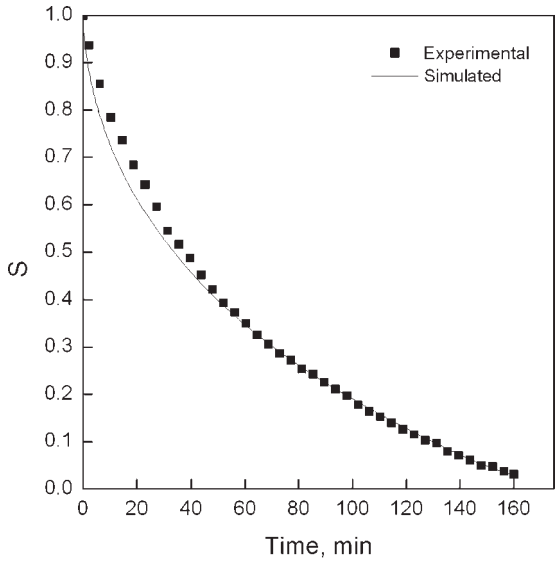

Figure 9. Predicted and measured drying curves for conventional freeze drying at 25°C.

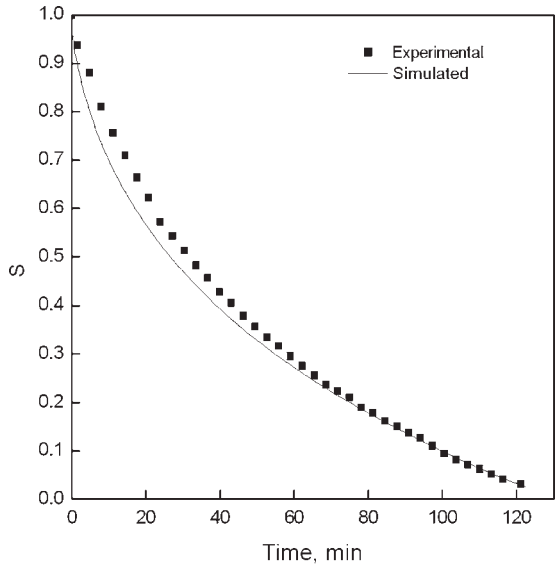

Figure 11. Predicted and measured drying curves for conventional freeze drying at 41°C.

For dielectric-material-assisted microwave freeze drying at 25°C, the value of the electric field strength had to be adjusted to get the best fit, since there was no way to measure the electric field strength in the microwave cavity of the apparatus directly. The electric field strength, E, used in the simulation was 3450 V/m after examination of a few values. Figure 10 displays an excellent fit, providing reasonable confidence that the assumed value of E was realistic. It should be noted that only this fitted parameter distinguished conventional freeze drying and dielectric-material-assisted microwave freeze drying at a given operating temperature.

Good agreement was also observed between the predicted and measured drying curves at 41°C. Figures 11 and 12 are for conventional freeze drying and dielectric-material-assisted microwave freeze drying, respectively. An average pore radius, $\bar{r}$, of 2.5×10^{-6} m was used here instead of 2.65×10^{-6} m, while α was set equal to 2 as in the previous simulation. This substitution was made to improve the fit. This suggests that the ratio in the proposed equilibrium relation of Eq. 21 may depend in some way on temperature. By and large, the proposed relation was successful in quantifying the hygroscopic effect. Exactly how the equilibrium relation works with other materials has to be determined with experiments. The trend is that the more hygroscopic the material, the smaller the value of α; the less hygroscopic the material, the larger the value of α.

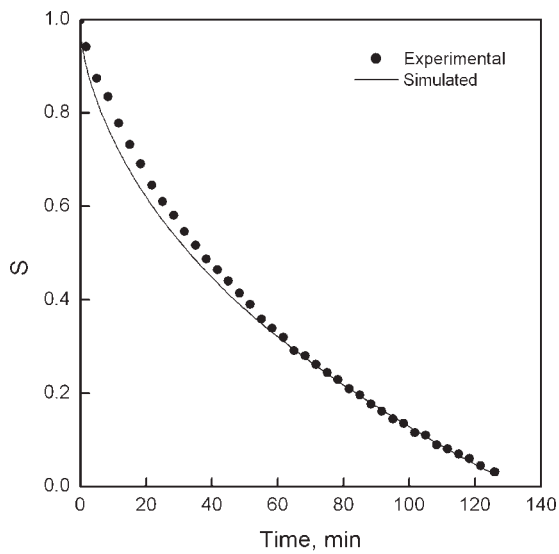

Figure 10. Predicted and measured drying curves for dielectric-material-assisted microwave freeze drying at 25°C.

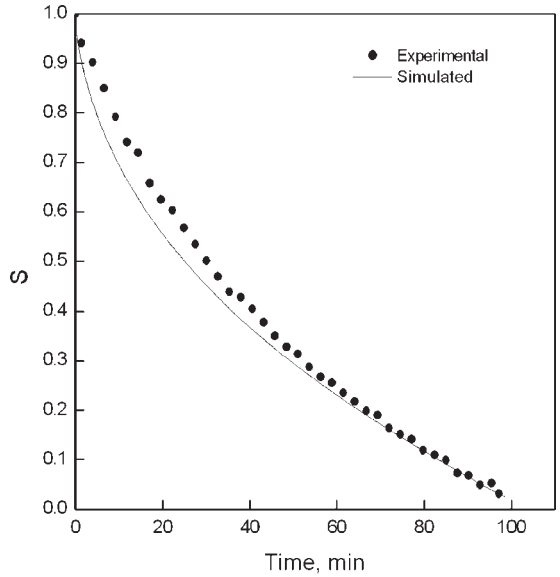

Figure 12. Predicted and measured drying curves for dielectric-material-assisted microwave freeze drying at 41°C.

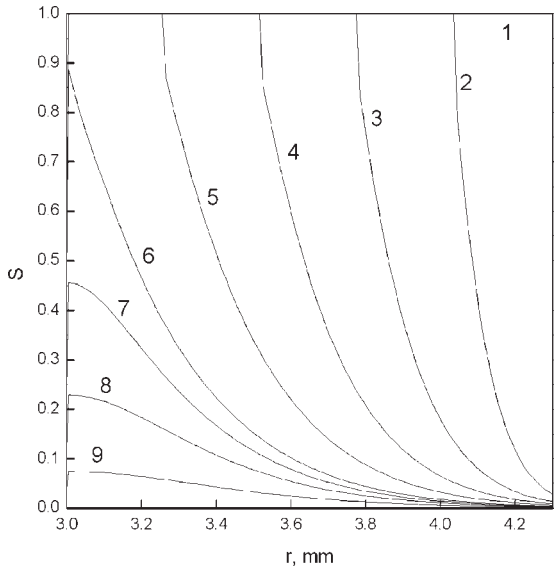

Figure 13. Profile of ice saturation within a sample at 25°C.

The common feature of Figures 9–12 is that the predicted drying rate decreased faster than was experimentally observed in the early stage of drying, i.e. the primary drying stage. These initial slight overpredictions may be due to the slightly lower pressure used than the actual value that the sample experienced. For the same reason, the slightly underestimated predictions using at the slightly high ambient pressure in the later drying stages gradually brings the theoretical results back to the real rate.

Effect of the dielectric material

The good agreements achieved between the model predictions and the experimental measurements for conventional freeze drying and dielectric-material-assisted microwave freeze drying certainly provide an indication that the mathematical model is realistic. Although the experiment of microwave freeze drying without the assistance of the dielectric material could not be carried out, theoretical predictions can now be made with a reasonable accuracy. Using the conditions of Figure 10 but replacing the SiC rod with a quartz rod, the predicted drying curve of ordinary microwave freeze drying was so close to that for conventional freeze drying that they almost collapse into one curve. This doubly confirms that the dielectric material can indeed significantly enhance microwave freeze drying. In other words, microwave heating can only be helpful in freeze drying when dielectric materials are employed if the solute has a small loss factor or solid content in solution is low.

Profiles of ice saturation and temperature

There are totally four variables governing the freeze drying process, i.e., temperature, ice saturation, vapor concentration, and pressure besides the spatial and time variables. Two of them are dependent because they are restricted by the ideal gas law and the adsorption equilibrium relationship. Temperature and ice saturation were selected as the primary variables to correspond to heat and mass transfer equations. Since the profiles of these two variables at 25°C and 41°C are similar, only the case at 25°C is presented here.

Figure 13 illustrates ice saturation profile within a sample during drying. In the primary drying stage, the sublimation front gradually recedes into the sample from the material surface. There is still a certain amount of moisture remaining in the drying region due to the adsorption–desorption equilibrium. The magnitude of the ice saturation depends on the local temperature and pressure. At a drying time of 95.2 min, the primary drying stage ends as the sublimation front reaches the surface of the dielectric material core, and the secondary drying stage starts. In the secondary drying stage, moisture removal comes mostly from the surface sublimation of adsorbed moisture. It can be seen that saturation in the drying region gradually decreases with time. The drying process ceases when the average residual ice saturation is less than a final value required with the overall drying time being 126.7 min.

Figure 14 shows the temperature profile within a sample during drying. Dielectric-material-assisted microwave heating is seen to take place throughout the drying process. At the beginning of drying, the surface temperature suddenly drops to a very low value, a phenomenon commonly encountered in freeze drying. A gradual decrease in temperature from the core surface to the sublimation front in the initial 95.2 min of drying indicates that the heat needed for front sublimation mainly comes from the dielectric material core through conduction. The uniform temperature distribution within the core is a result of the very high thermal conductivity of the dielectric material as discussed previously. The drying rate-controlling factor is the resistance to vapor movement from the sublimation front to the sample surface. After the start of the secondary stage, the material temperature rises quickly, since removal of the bound water through desorption requires a higher temperature to promote the internal phase change. Heat transfer becomes the rate-controlling step during this stage. In the late stage of drying, radiation from the sur-

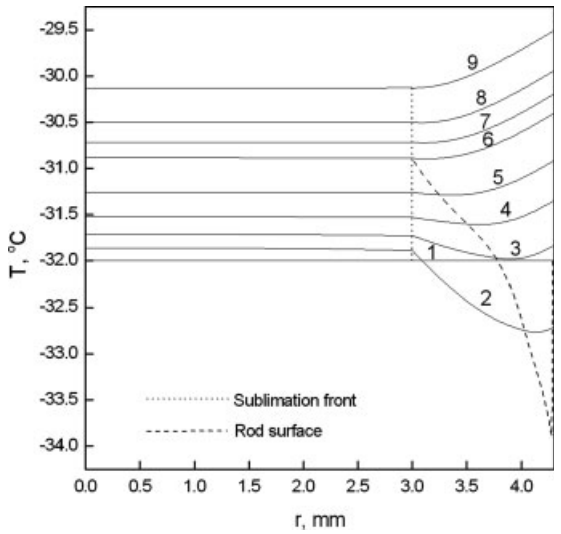

Figure 14. Profile of temperature within a sample at 25°C.

roundings also plays an important role in heat transfer. The highest material temperature is predicted to occur on the sample surface at the end of drying. This is because of the low electric field strength used in the present simulation. It is believed that a lower operating pressure should allow a higher microwave power input to shorten the drying time, which will be demonstrated by both experiment and simulation.

Conclusion

A laboratory scale microwave freeze drying apparatus was developed aimed at experimentally verifying the beneficial effect of a dielectric material on freeze drying with microwave heating. Sintered SiC was used as the dielectric material. Mannitol, a typical pharmaceutical excipient, was selected as the solute in aqueous solution. The experimental results show that the use of the dielectric material in microwave freeze drying can effectively enhance the freeze drying rate. More than 20% of drying time was saved compared with conventional freeze drying under the operating conditions tested. A porous media mathematical model of freeze drying with hygroscopic effect was derived and solved numerically using the finite difference method with a moving boundary. The hygroscopic effect was quantified based on a modified adsorption–desorption relationship. For mannitol, the ratio of vapor pressures between the adsorption–desorption equilibrium and the thermodynamic equilibrium follows the square root of the moisture saturation. Comparisons of drying curves between experimental data and theoretical predictions displayed good agreements. Simulation results also show that when the solid content of the solution to be freeze dried is very low or the solid product has a very small loss factor, microwave heating is less effective unless dielectric materials are employed. Drying rate controlling factor was analyzed to be mass transfer in the primary drying stage and heat transfer in the secondary drying stage.

Acknowledgments

The financial support of Hong Kong's Research Grants Council through grants HKUST 600704/C4586 and HKUST 6038/00P are gratefully acknowledged.

Notation

a = coefficients in the discretization equation
b = source-term in the discretization equation
c = specific heat capacity, J/(kg K)
d_p = diameter of the dielectric material core, m
D = diffusivity, m^2/s
D_p = diameter of the frozen material, m
e = emissivity
E = electric field strength, V/m
F = angle factor
ΔH = latent heat, J/kg
j = mass flux, kg/(m^2 s)
k = microwave energy dissipation coefficient, $W/m^3 \cdot (V/m)^{-2}$
K_D = permeability, m^2
K_r = relative permeability
K_S = effective diffusivity by saturation gradient, kg/(m s)
K_T = effective mass conductivity by temperature gradient, kg/(m s K)
M_w = molecular weight of water vapor, kg/kg mol
n_D = node number for the vapor concentration calculation in each time step
n_S = node number for the saturation calculation in each time step
n_T = node number for the temperature calculation in each time step
P = pressure, Pa
P_v = saturated pressure of vapor, Pa
q = heat flux, J/(m^2 s)
$\dot{q}$ = internal heat generation intensity, W/m^3
r = spatial axis, m
r_p = radius of the dielectric material core, m
$\bar{r}$ = average pore radius in the solid matrix, m
R = spatial position of the sublimation front, m
R_p = material radius, m
R_v = gas constant of water vapor, $m^2/(s^2 K)$
R^- = spatial position close to front from inside, m
R^+ = spatial position close to front from outside, m
S = moisture saturation
S_C = constant part of the source-term expression
S_{ini} = initial saturation after sublimation front movement
S_P = coefficient of the source-term expression
S_t = source-term expression
t = time, minute
T = temperature, K
W = weight, kg
X = moisture content on dry base

Greek letters

α = parameter in the adsorption equation
ε = porosity
φ = diameter, m
Φ = generalized dependent variable in the discretization equation
λ = thermal conductivity, J/(m·s·K)
μ = dynamic viscosity, kg/(m·s)
ρ = density, kg/m^3
σ = Stefan–Boltzmann constant, $W/(m^2 K^4)$
τ = tortuosity

Subscripts

0 = initial value
amb = ambient value
avg = average
E = east end point in a grid
i = ice
l = node number in calculation
m = dielectric material
P = grid node
s = solid matrix
sf = of the sublimation front
v = vapor
W = west end point in a grid
t = total

Superscript

j = iteration number in calculation

Literature Cited

1. Oetjen GW, Haseley P. *Freeze Drying*, 2nd ed., Weinheim: Wiley-VCH, 2004.
2. Dolan JP, Scott EP. Microwave freeze-drying of aqueous solutions. In: Hayea LJ, Roemer RB, editors. *Advances in Heat and Mass Transfer in Biological Systems ASME*, HTD-Vol. 288. New York: United Engineering, 1994:91–98.
3. Adams GDJ. Freeze-drying of biological materials. *Drying Technol*. 1991;9:891–925.
4. Choi MJ, Briancon S, Andrieu J, Min SG, Fessi H. Effect of freeze-drying process conditions on the stability of nanoparticles. *Drying Technol*. 2004;22:335–346.
5. Liapis AI, Bruttini R. Freeze drying. In: Mujumdar AS, editor. *Handbook of Industrial Drying*, Vol. 2, New York: Marcel Dekker, 2nd ed., 1995:305–343.

6. Wang W, Chen G. Numerical investigation on dielectric material assisted microwave freeze-drying of aqueous mannitol solution. *Drying Technol*. 2003;21:995–1017.
7. Ma YH, Peltre PR. Freeze dehydration by microwave energy. II. Experimental investigation. *AIChE J*. 1975;21:344–350.
8. Ang TK, Pei DCT, Ford JD. Microwave freeze drying: an experimental investigation. *Chem Eng Sci*. 1977;32:1477–1489.
9. Wang ZH, Shi MH. Effects of heating methods on vacuum freeze drying. *Drying Technol*. 1997;15:1475–1498.
10. Wang ZH, Shi MH. Microwave freeze drying characteristics of beef. *Drying Technol*. 1999;17:433–447.
11. Ben Souda K, Akyel C, Bilfen E. Freeze dehydration of milk using microwave energy. *J Microw Power Electromagn Energy*. 1989;24: 195–202.
12. Wang W, Chen G, Gao F. Effect of dielectric material on microwave freeze-drying of skim milk. *Drying Technol*. 2005;23:317–340.
13. Wang W, Chen G. Heat and mass transfer in dielectric-material-assisted microwave freeze-drying of skim milk with hygroscopic effect. *Chem Eng Sci*. 2005;60:6542–6550.
14. Wang W, Chen G. Theoretical study on microwave freeze-drying of an aqueous pharmaceutical excipient with the aid of dielectric material. *Drying Technol*. 2005;23:2147–2168.
15. Basak T, Priya AS. Role of ceramic supports on microwave heating of materials. *J Appl Phys*. 2005;97:1–12.
16. Basak T, Priya AS. Role of metallic and ceramic supports on enhanced microwave heating processes. *Chem Eng Sci*. 2005;60: 2661–2677.
17. Basak T, Aparna K, Meenakshi A, Balakrishnan AR. Effect of ceramic supports on microwave processing of porous food samples. *Int J Heat Mass Transfer*. 2006;49:4325–4339.
18. Basak T, Meenakshi A. A theoretical analysis on microwave heating of food slabs attached with ceramic plates: role of distributed microwave incidence. *Food Res Int*. 2006;39:932–944.
19. Tang X, Pikal MJ. Design of freeze-drying processes for pharmaceuticals: practical advice. *Pharm Res*. 2004;21:191–200.
20. Wu HW, Tao Z, Chen G, Deng HW, Xu GQ, Ding ST. Conjugate heat and mass transfer process within porous media with dielectric cores in microwave freeze drying. *Chem Eng Sci*. 2004;59:2921–2928.
21. Tao Z, Wu H, Chen G, Deng H. Numerical simulation of conjugate heat and mass transfer process within cylindrical porous media with cylindrical dielectric cores in microwave freeze-drying. *Int J Heat Mass Transfer*. 2005;48:561–572.
22. Snowman JW. Formulation and cycle development for lyophilization: first steps. *Pharm Eng*. 1993;13:26–34.
23. Hatley RHM, Franks F. Application of DSC in the development of improved freeze-drying process for labile biologicals. *J Therm Anal*. 1991;37:1905–1914.
24. Whitaker S. Simultaneous heat, mass, momentum transfer in porous media: a theory of drying. *Adv Heat Transfer*. 1977;13:119–203.
25. Geankoplis CJ. *Transport Processes and Unit Operations*, 3rd ed., NJ: Englewood Cliffs, 1993:462–466.
26. Liapis AI, Bruttini RA. Theory for the primary and secondary drying stages of the freeze-drying of pharmaceutical crystalline and amorphous solutes: comparison between experimental data and theory. *Sep Technol*. 1994;4:144–155.
27. Nield DA, Bejan A. *Convection in Porous Media*, New York: Springer, 1992:45.
28. Do DD. *Adsorption Analysis: Equilibria and Kinetics*, *Series on Chemical Engineering*, Vol. 2, London: Imperial College Press, 1998:188–190.
29. Ni H, Datta AK, Tottance KE. Moisture transport in intensive microwave heating of biomaterials: a multiphase porous media model. *Int J Heat Mass Transfer*. 1999;42:1501–1512.
30. Chen GH, Wang W, Mujumdar AS. Theoretical study of microwave heating patterns on batch fluidized bed drying of porous material. *Chem Eng Sci*. 2001;56:6823–6835.
31. Bird RB, Stewart WE, Lightfoot EN. *Transport Phenomena*, 2nd ed., New York: Wiley, 2002;488–508.
32. Echert ERG, Drake RM. *Analysis of Heat and Mass Transfer*, New York: McGraw-Hill, 1987:767–783.
33. Munro RG. Material properties of a sintered alpha-SiC. *J Phys Chem Ref Data*. 1997;26:1195–1203.
34. Liley PE. Physical and chemical data, In: Perry HR, Green DW, Maloney JO, editors. *Perry's Chemical Engineers' Handbook*, 7th ed., New York: McGraw-Hill, 1997:2–40, 2–176, 2–304.
35. Meredith R. *Engineers' Handbook of Industrial Microwave Heating*. London: The Institution of Electrical Engineers, 1998.
36. Sadikoglu H, Liapis AI. Mathematical modeling of the primary and secondary drying stages of bulk solution freeze-drying in trays: parameter estimation and model discrimination by comparison of theoretical results with experimental data. *Drying Technol*. 1997;15:791–810.
37. Idelchik IE. General information and element of aerodynamics and hydraulic of pressure systems. In: Steinberg MO, Malyavskaya GR, Martynenko OG, editors. *Handbook of Hydraulic Resistance*, 3rd ed., Florida: CRC press, 1994:9–12.
38. Patanker SV. *Numerical Heat Transfer and Fluid Flow*, New York: Hemisphere Publishing. 1980:48–49, 67–68.

Manuscript received Feb. 15, 2007, and revision received July 4, 2007.